Nanoscale

RSC Publishing

PAPER

View Article Online
View Journal | View Issue

Cite this: *Nanoscale*, 2013, **5**, 5841

Simultaneous SERS detection of copper and cobalt at ultratrace levels

Dionysia Tsoutsi,[abc] Luca Guerrini,[abc] Jose Manuel Hermida-Ramon,[a] Vincenzo Giannini,[d] Luis M. Liz-Marzán,[aef] Alexander Wei*[g] and Ramon A. Alvarez-Puebla*[abch]

Received 27th March 2013
Accepted 17th April 2013

DOI: 10.1039/c3nr01518a

www.rsc.org/nanoscale

We report a SERS-based method for the simultaneous and independent determination of two environmental metallic pollutants, Cu(II) and Co(II). This was achieved by exploiting the coordination-sensitive Raman bands of a terpyridine (TPY) derivative for detecting transition metal ions. Changes in the vibrational SERS spectra of dithiocarbamate anchored terpyridine (TPY-DTC) were correlated as a function of each metal ion concentration, with limits of detection comparable to those of several conventional analytical methods. Simultaneous detection of ultratrace levels of Co(II) in the presence of high Cu(II) concentration was also demonstrated, supporting the potential of this sensing strategy for monitoring potable water supplies.

Introduction

Quantitative detection of metal ions in solution at trace levels is a topic of widespread interest, spanning from environmental sensing in natural waters through industrial process monitoring to biomedical diagnostics. Traditionally, the most common analytical techniques employed for these purposes are atomic absorption or emission spectroscopy,[1] but these are destructive and cannot be implemented for remote sensing. Also, pre-concentration procedures are necessary when dealing with ultralow concentrations, which require substantial amounts of sample to achieve passable levels of detection.[2,3] Newer analytical strategies based on optical methods have been developed to overcome these problems.[4,5] Optical detection modalities include the ratiometric fluorescence emission of organic fluorophores[6] or quantum dots[7] and adsorbate-induced shifts in the plasmonic signature of noble metal nanoparticles.[8]

Recently, it has been shown that surface-enhanced Raman scattering (SERS) spectroscopy can support the rapid and ultrasensitive detection of specific analytes in aqueous solution and complex media.[9,10] Unlike the broad, structureless signals from fluorescence and plasmon-resonant extinction, SERS is a spectroscopic sensing modality that can support analyte detection based on their unique Raman fingerprint. However, SERS cannot directly detect monoatomic species that lack vibrational signatures, unless they are chemically bound to the SERS substrate.[11] As an alternative, metal ions can be detected either by (i) binding to an organic receptor ligand whose SERS profile can be modulated by formation of a coordination complex,[11–17] or (ii) indirect detection using particles encoded with Raman reporters whose SERS intensities are selectively perturbed by complexation of the target ions, either through surface-bound receptors (*e.g.*, peptides[18] and DNA strands[19,20]) or by direct adsorption onto the plasmon-active surface.[21] The latter approach can provide sensitivities at the nanomolar level, but has inherent limitations for distinguishing multiple ions. In contrast, the use of chemoselective receptors bound to plasmonically active substrates is capable of yielding intense SERS signals with characteristic spectral "fingerprints" produced by their interaction with different ions, and thus offers greater potential for multiplex detection.[16] Additionally, the organic ligands can serve as internal standards that ensure the reliability of the SERS sensing platform, and the analytical range of response can be easily controlled by varying the amount of chemoreceptor available on the metal surface.[13]

With respect to the choice of metal-ion receptors, terpyridines are particularly appealing ligands because they bind metal ions *via* Raman-active pyridine units.[14,22,23] For a given terpyridine (TPY) structure, the conformation and electronic structure of the ligand–metal complex depend strongly on the metal ion species.[22,23] Furthermore, the TPY binding site can be

[a]*Departamento de Química Física, Universidade de Vigo, 36310, Vigo, Spain. E-mail: ramon.alvarez@ctqc.org; ramon.alvarez@urv.cat*

[b]*Departamento de Ingenieria Electronica, Universitat Rovira i Virgili, Avda. Països Catalans 26, 43007 Tarragona, Spain*

[c]*Centro de Tecnologia Quimica de Cataluña, Carrer de Marcel li Domingo s/n, 43007 Tarragona, Spain*

[d]*Department of Physics, Imperial College London, London SW7 2AZ, UK*

[e]*Bionanoplasmonics Laboratory, CIC biomaGUNE, Paseo de Miramón 182, 20009 Donostia –San Sebastián, Spain*

[f]*Ikerbasque, Basque Foundation for Science, 48011 Bilbao, Spain*

[g]*Department of Chemistry, Purdue University, 560 Oval Drive, West Lafayette, Indiana 47907-2084, USA. E-mail: alexwei@purdue.edu*

[h]*ICREA, Passeig Lluís Companys 23, 08010 Barcelona, Spain*

easily oriented toward the bulk solution for the facile capture of metal ions by introducing, as we describe here, a dithiocarbamate (DTC) unit at the opposite end of the TPY moiety, which functions as a robust anchoring group on the noble metal substrates[14,24,25] (the final product is referred to as TPY-DTC).

Here we show that the coordination properties of TPY ligands permit the simultaneous determination of two metal pollutants, Cu(II) and Co(II),[26,27] in the ppb to ppt range using SERS. Although both Cu(II) and Co(II) are bioessential trace elements,[28] they are toxic at higher concentrations.[29,30] Over time, the long-term exposure of organisms to low amounts of these metal ions can result in a bioaccumulation to toxic levels, potentially promoting teratogenic or carcinogenic effects.[31] Thus, the development of accurate and sensitive field analysis for their quantitative monitoring in natural waters is of particular interest.

Experimental

Chemicals

All chemicals were purchased from Aldrich and used without further purification. Water was purified using a Milli-Q system (Millipore). 4′-(*N*-Piperazinyl)terpyridine (pTPY) was synthesized as previously reported[14,32] by condensing 4′-chloroterpyridine with piperazine in 2,6-lutidine for 24 h at 130 °C in a sealed reaction tube. pTPY was converted to the corresponding dithiocarbamate salt (TPY-DTC) by treatment with 1 equivalent each of CS_2 and Et_3N in 1 : 1 CH_2Cl_2–MeOH, and used without further purification (final TPY-DTC concentration = 0.5 mM).

Nanoparticle synthesis and functionalization

Ag nanoparticles were prepared *via* the method reported by Lee and Meisel.[33] Briefly, 2 mL of 1 wt% sodium citrate solution was added to 100 mL of a 1 mM solution of $AgNO_3$ at reflux and stirred for 1 hour. The resulting colloidal solution had a turbid gray-green colour. For functionalization, the Ag nanoparticles were centrifuged for 10 min at 2200 rcf, then decanted and redispersed in ethanol (2.5 times the retentate volume) before treatment with a TPY-DTC solution in 1 : 1 CH_2Cl_2–MeOH (final TPY-DTC concentrations of 10^{-5}, 10^{-6} and 10^{-7} M). TPY-DTC ligands were allowed to adsorb overnight onto the Ag nanoparticles. 500 μL of the as-prepared TPY-DTC nanoparticle dispersion was then added to aqueous solutions containing different amounts of Co(II) and Cu(II), and gently stirred for 3 hours. Afterwards, 40 μL of the colloidal mixture was cast, air-dried, and analyzed by SERS.

Computational analysis

The geometries of the ligand and metal complexes with several water molecules were optimized by density functional theory (DFT) using the B3LYP functional with 6-31+G* basis set. Silver atoms were described by the LANLDZ effective core potential together with the corresponding basis set. Frequency and force constants were obtained to enable a detailed vibrational assignment. Near field enhancement calculations, *i.e.* the near field intensity normalized by the incident intensity, were performed by using a 3D formulation of the scattering equations with the Green method.[34]

Instrumentation

UV-vis-NIR spectra were recorded using an Agilent 8453 diode array spectrophotometer. Transmission electron microscopy (TEM) was carried out using a JEOL JEM 1010 microscope operating at an acceleration voltage of 100 kV. Raman and SERS experiments were conducted using a Renishaw InVia Reflex confocal microscope equipped with a 50× objective and a high-resolution grating with 1200 grooves per cm for NIR wavelengths, additional band-pass filter optics, and a 2D-CCD camera. SERS spectra were acquired using 785 nm excitation with exposure times of 10 s.

Results and discussion

TPY ligands have high affinity for first-row transition metal ions such as Co(II) and Cu(II). The metal-chelating domain of the TPY structure comprises three nearly coplanar sp^2 nitrogen atoms, capable of supporting dπ–pπ* back-bonding with the chelated metal ion.[35] The TPY ligand reorganizes from a *transoid* to *cisoid* conformation upon metal coordination (Fig. 1A; 4′-(*N*-piperazinyl)terpyridine, pTPY).[36] The effect of this conformational change on the photophysical properties of TPY is highly dependent on the nature of the metal ion, as indicated by the different electronic absorption profiles of its coordination complexes in solution (Fig. 1B). Although all three species exhibit a strong absorption band around 280 nm due to the

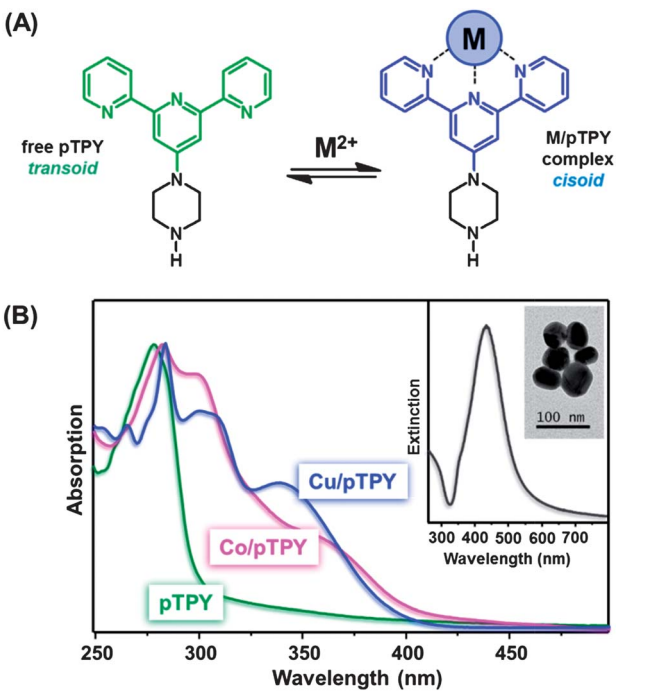

Fig. 1 (A) Chemical structures of a free pTPY receptor and the one coordinated to a metal ion (green and blue respectively). (B) Normalized electronic absorption spectra of free pTPY and its equimolar Co(II) and Cu(II) complexes in 1 : 1 CH_2Cl_2–MeOH. Inset: A TEM image and an extinction spectrum of colloidal silver.

π–π* transitions of the TPY chromophore, both the Cu(II)–pTPY and Co(II)–pTPY complexes display a bathochromic shift relative to the free ligand (maxima at 283 and 282 nm, respectively). This, along with the characteristic metal-to-ligand charge transfer band (310, 339 nm for Cu; 302, 360 nm for Co), is typical for TPY–transition metal complexes.[37]

Consistent with its electronic absorption, the Raman bands of the TPY moiety, whose vibrational assignment was based on density functional theory (DFT) calculations, are also strongly affected by metal coordination (Fig. 2). Theoretical calculations of the Raman spectra for the free and metal-bound pTPY ligand (prior to DTC functionalization) were performed to identify the vibrational contributions specific to the TPY unit. The effects of Co(II) and Cu(II) ion complexation on the TPY Raman bands are similar for both complexes in the 1300–1650 cm^{-1} region. Upon coordination, this region is characterized by a general broadening of the Raman peaks assignable to ring stretching modes and other in-plane deformations: 1606 cm^{-1}, which is the result of several contributions ascribed to ν(CC) and ν(CN) ring modes of the three pyridine units; 1474 cm^{-1}, due to a combination of a ν(CNC) in-plane ring and the CH in plane deformations; and a new band arising at 1324 cm^{-1}, attributed to the CH rocking and the complex ν(CN) and ν(CC) inter- and intra-ring modes. However, in the 1200–1300 cm^{-1} region, the intense sharp features of the free TPY ligand weaken to yield a single broad and weak band for Co–pTPY and Cu–pTPY approximately centered at 1243 cm^{-1}.

The most sensitive change in the TPY Raman spectra upon metal coordination is observed in the ring-breathing bands around 1000 cm^{-1}. In the solid state, the doublet at 988 and 994 cm^{-1} of the free pTPY ligand undergoes a marked shift upon complexation with Co(II) to give an intense peak centered at 1017 cm^{-1}, with two visible shoulders at 1005 cm^{-1} and 1028 cm^{-1}. Cu(II) coordination to the TPY moiety also produces three well-resolved bands that are distinct from both free pTPY or Co(II)–pTPY, with the most intense peak at 1019 cm^{-1} and two more at 997 and 1038 cm^{-1}. These differences in the solid-state Raman profiles of Co(II)–pTPY and Cu(II)–pTPY are also observed in the SERS spectra of the metal–TPY-DTC complexes (see below), and are sufficient to determine the identity of the analytes of interest. It is worth noting that other spectral differences can also contribute toward the distinction between Co(II)–TPY and Cu(II)–TPY: for instance, Cu(II) complexation produces several weak bands in the fingerprint region between 1064 and 1366 cm^{-1} that are not present in either the free pTPY or Co(II)–pTPY Raman spectra.

The TPY ligands were anchored onto colloidal Ag nanoparticles (NPs; d = 30–60 nm; Fig. 1B, inset) using *in situ* DTC formation (see the Experimental section). The TPY-DTC functionalized NPs formed stable dispersions in aqueous solutions, with strong SERS activities at 785 nm. To optimize the sensing performance of the substrates, we first studied the effects of molecular crowding at the metal surface on the structural properties of the self-assembled TPY-DTC receptors. Fig. 3 illustrates the SERS spectra of Ag NPs treated with TPY-DTC

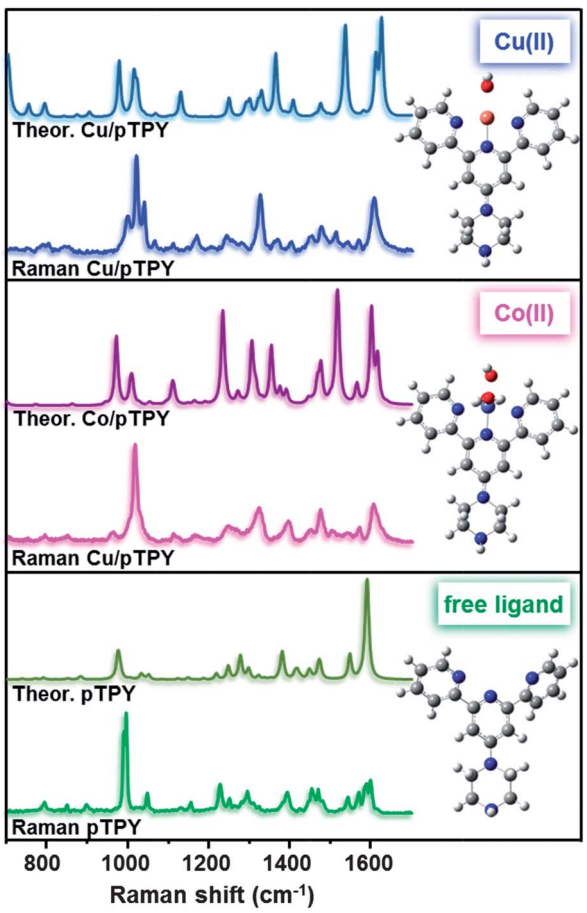

Fig. 2 Comparison of theoretical and experimental (solid-state) Raman spectra of pTPY and its metal complexes. The geometries of pTPY and its complexes (with added water molecules) were optimized by DFT-B3LYP calculations using the 6-31+G* basis set. Raman spectra were obtained using 785 nm excitation.

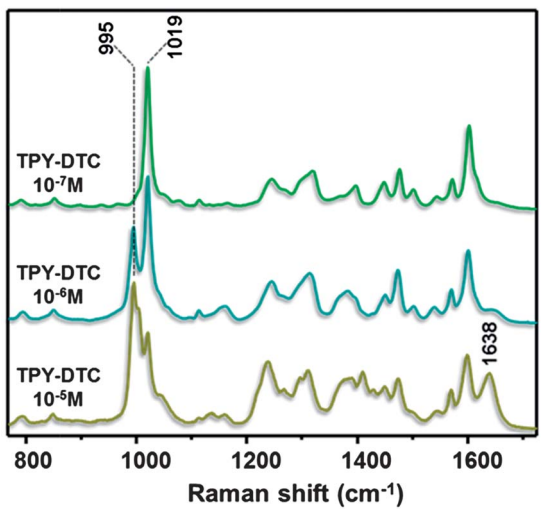

Fig. 3 SERS spectra of TPY-DTC anchored onto Ag NPs as a function of free ligand concentration. Different aliquots of TPY solutions were added to Ag nanoparticles dispersed in ethanol (~6 × 10^{10} NPs per mL) until the desired final concentrations were obtained (10^{-5} to 10^{-7} M). An aliquot of TPY-DTC–Ag NPs was diluted in deionized water before being cast, air-dried, and analyzed by SERS at 785 nm.

solutions at concentrations ranging from 10^{-5} to 10^{-7} M, which is the practical sensitivity limit. As can be observed, higher adsorbate concentrations result in significant spectral changes, presumably related to increases in ligand surface densities. In particular, the narrow ring-breathing mode at 1019 cm^{-1} for TPY-DTC at 10^{-7} M was split into a second contribution at 995 cm^{-1}, and a new feature at 1638 cm^{-1} arises in the spectral region characteristic of the ν(CN) and ν(CC) stretching modes. These results suggest that the structural and electronic properties of the conjugated π-system in TPY are significantly influenced by the ligand surface density, due to lateral interactions between molecules at high surface crowding. Such changes in the conformational distribution of the TPY unit can affect its ability to coordinate to metal ions. In this regard, Traulsen *et al.*[38] recently showed that the amount of Pd(II) captured by a monolayer of TPY ligands on a metal substrate does not correlate well with the number of host binding sites. Instead, the metal coordination efficiency improves with a reduction in TPY density. For this reason, 10^{-7} M was selected as the optimum TPY-DTC concentration for Ag NP functionalization. Consequently, the dynamic range for metal ion detection by SERS was optimized by adjusting the Ag NP concentration, rather than by varying the density of binding sites per nanoparticle.

The SERS spectra of TPY-DTC–Ag NPs were then recorded in the presence of varying amounts of Co(II) and Cu(II) (selected spectra in Fig. 4). NP dispersions were combined with aliquots of $CoCl_2$ and $CuCl_2$ solutions and gently agitated for three hours before drop-casting onto a Si wafer for SERS analysis (see the Experimental section). The coordination of metal ions to TPY-DTC ligands produced a general and non-specific red shift of several vibrational bands associated with in-plane ring vibrational modes, namely at 1318, 1474 and 1601 cm^{-1}. More importantly, analyte-specific changes were observed in the ring-breathing spectral region near 1000 cm^{-1}, indicative of TPY complexation with Co(II) or Cu(II). Concentrations of metal ions higher than those reported in Fig. 4 did not induce any further change of the ligand spectral profile.

To determine the utility of TPY-DTC–Ag NPs for ultratrace SERS detection of Co(II) and Cu(II), analyses were optimized as a function of NP concentration relative to analyte solutions. At relatively high metal ion concentrations (ppb levels), the vibrational peak of the metal–TPY-DTC complex (ν_{com} = 1033 cm^{-1} for Co(II), 1040 cm^{-1} for Cu(II)) increases at the expense of the uncomplexed TPY vibrational mode (ν_{free} = 1019 cm^{-1}; Fig. 5A). These changes were correlated quantitatively with metal ion concentration using ratiometric peak intensities, I_{com}/I_{free}. Spectral peak deconvolution was performed for each Raman band between 1019 and 1040 cm^{-1} at fixed FWHM values with the assumption of Lorentzian lineshapes.[39] A plot of I_{com}/I_{free} *versus* analyte concentration reveals a linear correlation for both Co(II) and Cu(II) (r^2 > 0.97; Fig. 5B–D). The detection limit is 6.5 ppb for Cu(II), and 60 ppt for Co(II). These values are at the same level or even lower than those obtained by widely accepted methods such as ICP (0.3 ppm for Cu) or FAAS (0.5 ppm for Cu, and 50 ppb for Co), and are competitive with ICP-MS (0.1 ppb for Cu, and 40 ppt for Co).[27,40]

It is worth noting that a marked aggregation of TPY-DTC–Ag NPs was observed upon addition of Co(II), even at low analyte concentrations. This can be attributed to the supramolecular

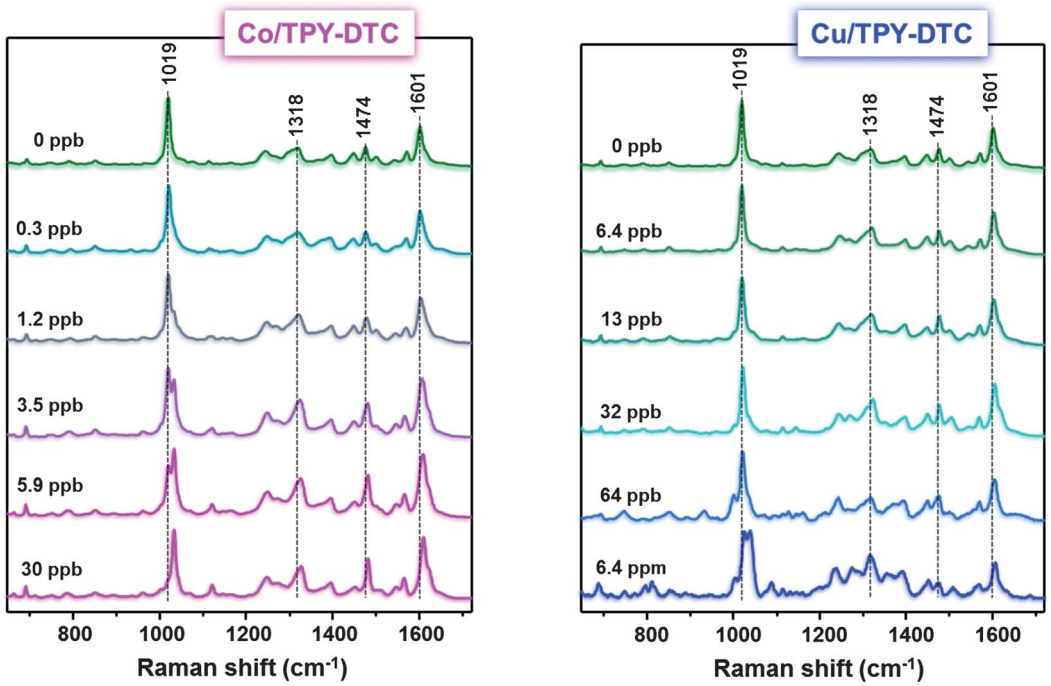

Fig. 4 SERS spectra of TPY-DTC anchored onto Ag NPs at variable concentrations of $CoCl_2$ and $CuCl_2$. Ag NPs functionalized with TPY-DTC (10^{-7} M) were added to aqueous solutions containing different amounts of Co(II) and Cu(II) and gently stirred for 3 hours; 40 μL of each mixture was then cast, air-dried, and analyzed by SERS.

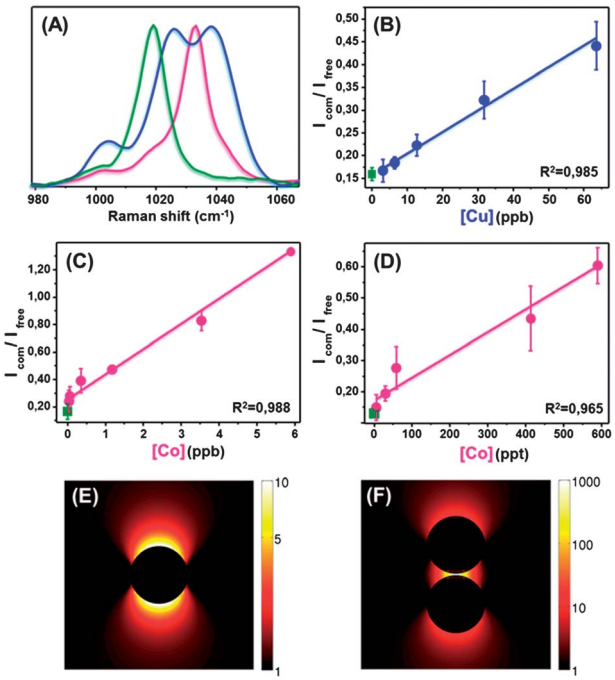

Fig. 5 (A) Analyte-sensitive bands in the normalized SERS spectra of TPY-DTC in the absence of transition-metal ion (green line), in the presence of Co(II) (30 ppb, pink line), and in the presence of Cu(II) (6.4 ppm, blue line). (B) I_{com}/I_{free} as a linear function of [Cu], with a limit of detection at 6.5 ppb. (C and D) I_{com}/I_{free} as a linear function of [Co], with a limit of detection at 60 ppt. The concentration of TPY-functionalized Ag NPs in sample (D) is ten times lower than in (B) and (C); error bars equal to two standard deviations ($N = 5$). (E and F) Near-field intensity maps ($\log_{10}$ scale normalized to the incident field) for 45 nm Ag NP spheres at 785 nm excitation: (E) a single Ag NP; (F) a NP dimer with 2 nm gap.

formation of bidentate $[Co(TPY)_2]^{2+}$ bridges between nanoparticles, as the stability constants for metal–TPY complexes increase with the degree of coordination (β_1(Co–TPY) > 10^8; β_2(Co–TPY) > 10^{10}).[41–43] This is also consistent with the observation that the colloidal solutions remain stable at higher Co(II) concentrations, due to the saturation of the TPY ligands. In contrast, nanoparticles were not destabilized by Cu(II), regardless of concentration. This result was again expected, since β_1(Cu–TPY) ~ β_2(Cu–TPY) ~ 10^8, permitting an exchange between non-bridging $[Cu(TPY)]^{2+}$ and bridging $[Cu(TPY)_2]^{2+}$ complexes.[41,44] The formation of the bidentate $[Co(TPY)_2]^{2+}$ bridges between nanoparticles generates uniform hot spots (interparticle separation ≤ 2 nm),[31] selectively enhancing signals of the metal–ligand complexes within the interparticle gap where the highest electromagnetic fields are concentrated. This accounts for the much higher sensitivity (nearly two orders of magnitude) of the TPY-based sensor for Co(II) detection as compared to Cu(II). The effect of localized electromagnetic fields on SERS signals is illustrated in Fig. 5E and F, where theoretical simulations of near-field intensity for a single Ag NP and its homodimer (45 nm spheres, 2 nm gap, λ = 785 nm) are depicted.

The simultaneous detection of Co(II) and Cu(II) ions by TPY-DTC–Ag NPs may be useful for monitoring potable water supplies. Recent drinking water standards recommend maximum concentrations for Cu(II) and Co(II) of 250 ppm and 20 ppb, respectively.[45] To demonstrate the ability of our SERS-based method to detect ultratrace levels of Co(II) in the presence of high Cu(II) concentration, we designed an experiment using mixtures of each metal ion in variable amounts. Fig. 6 shows the SERS readout from the TPY-DTC–Ag NPs in the presence of Cu(II) and Co(II) at ppb levels. Most notably, SERS peaks corresponding to Co(II) adsorption can be distinguished at 0.6 ppb Co, and also in the presence of Cu(II) at a tenfold higher concentration. Similarly, Cu(II) can be detected in the presence of Co(II), but limited to a fivefold difference in concentration.

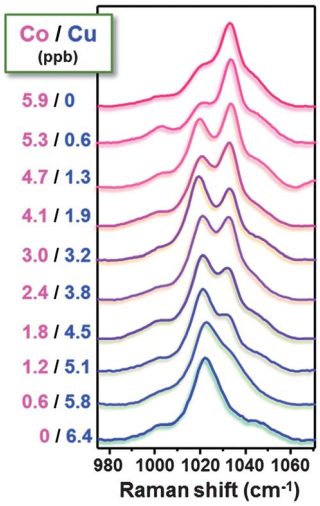

Fig. 6 Analyte-sensitive SERS bands from TPY-DTC–Ag NPs, after treatment with various mixtures of aqueous Co(II) and Cu(II) (listed in ppb).

Conclusions

In summary, we have engineered Ag nanoparticles into a quantitative, SERS-based sensor, using DTC-anchored terpyridine ligands with differential Raman spectral shifts in response to Co(II) and Cu(II). In the case of Co(II), the sensitivity of the TPY-DTC-coated Ag NPs toward these cations using SERS was significantly higher than that provided by conventional analytical methods such as AES and AAS. Further, the characteristic shifts in Raman peaks induced by each cation make it possible to provide a simultaneous and independent assessment of Co(II) and Cu(II).

Acknowledgements

D. T. acknowledges the financial support from the Universitat Rovira i Virgili. This work was funded by the Spanish Ministerio de Economía y Competitividad (CTQ2011-23167 and MAT2010-15374), the European Research Council (CrossSERS, FP7 MC-IEF 329131) and the U. S. National Science Foundation (CHE-0957738).

Notes and references

1 K. W. Jackson and T. M. Mahmood, *Anal. Chem.*, 1994, **66**, 252R–279R.

2 J. R. Chen and K. C. Teo, *Anal. Chim. Acta*, 2001, **450**, 215–222.
3 B. Godlewska-Zylkiewicz, *Microchim. Acta*, 2004, **147**, 189–210.
4 R. A. Sperling, P. Rivera gil, F. Zhang, M. Zanella and W. J. Parak, *Chem. Soc. Rev.*, 2008, **37**, 1896–1908.
5 D. J. de Aberasturi, J. M. Montenegro, I. R. de Larramendi, T. Rojo, T. A. Klar, R. Alvarez-Puebla, L. M. Liz-Marzan and W. J. Parak, *Chem. Mater.*, 2012, **24**, 738–745.
6 E. M. Nolan and S. J. Lippard, *J. Am. Chem. Soc.*, 2003, **125**, 14270–14271.
7 R. Freeman, T. Finder and I. Willner, *Angew. Chem., Int. Ed.*, 2009, **48**, 7818–7821.
8 F. Xia, X. L. Zuo, R. Q. Yang, Y. Xiao, D. Kang, A. Vallee-Belisle, X. Gong, J. D. Yuen, B. B. Y. Hsu, A. J. Heeger and K. W. Plaxco, *Proc. Natl. Acad. Sci. U. S. A.*, 2010, **107**, 10837–10841.
9 R. A. Alvarez-Puebla and L. M. Liz-Marzan, *Chem. Soc. Rev.*, 2012, **41**, 43–51.
10 L. Rodriguez-Lorenzo, L. Fabris and R. A. Alvarez-Puebla, *Anal. Chim. Acta*, 2012, **745**, 10–23.
11 R. A. Alvarez-Puebla and L. M. Liz-Marzan, *Angew. Chem., Int. Ed.*, 2012, **51**, 11214–11223.
12 R. A. Alvarez-Puebla and L. M. Liz-Marzan, *Energy Environ. Sci.*, 2010, **3**, 1011–1017.
13 D. Tsoutsi, J. M. Montenegro, F. Dommershausen, U. Koert, L. M. Liz-Marzan, W. J. Parak and R. A. Alvarez-Puebla, *ACS Nano*, 2011, **5**, 7539–7546.
14 Y. Zhao, J. N. Newton, J. Liu and A. Wei, *Langmuir*, 2009, **25**, 13833–13839.
15 S. W. Bishnoi, C. J. Rozell, C. S. Levin, M. K. Gheith, B. R. Johnson, D. H. Johnson and N. J. Halas, *Nano Lett.*, 2006, **6**, 1687–1692.
16 S. J. Lee and M. Moskovits, *Nano Lett.*, 2011, **11**, 145–150.
17 V. M. Zamarion, R. A. Timm, K. Araki and H. E. Toma, *Inorg. Chem.*, 2008, **47**, 2934–2936.
18 Z. Krpetic, L. Guerrini, I. A. Larmour, J. Reglinski, K. Faulds and D. Graham, *Small*, 2012, **8**, 707–714.
19 D. Han, S. Y. Lim, B. J. Kim, L. Piao and T. D. Chung, *Chem. Commun.*, 2010, **46**, 5587–5589.
20 Y. L. Wang and J. Irudayaraj, *Chem. Commun.*, 2011, **47**, 4394–4396.
21 G. Wang, C. Lim, L. Chen, H. Chon, J. Choo, J. Hong and A. J. deMello, *Anal. Bioanal. Chem.*, 2009, **394**, 1827–1832.
22 T. A. Laurence, G. B. Braun, N. O. Reich and M. Moskovits, *Nano Lett.*, 2012, **12**, 2912–2917.
23 T. A. Laurence, G. Braun, C. Talley, A. Schwartzberg, M. Moskovits, N. Reich and T. Huser, *J. Am. Chem. Soc.*, 2009, **131**, 162–169.
24 Y. Zhao, W. Perez-Segarra, Q. C. Shi and A. Wei, *J. Am. Chem. Soc.*, 2005, **127**, 7328–7329.
25 L. Guerrini, J. V. Garcia-Ramos, C. Domingo and S. Sanchez-Cortes, *Anal. Chem.*, 2009, **81**, 953–960.
26 I. C. Smith and B. L. Carson, *Trace Metals in the Environment*, 1981.
27 World Health Organization, *Guidelines for drinking-water quality* 2008.
28 A. W. Addison, W. R. Cullen, D. Dolphin and B. R. James, *Biological Aspects of Inorganic Chemistry*, 1977.
29 H. G. Seiler, A. Sigel and H. Sigel, *Handbook on metals in clinical and analytical chemistry*, Marcel Dekker, Inc., 1994.
30 G. Nordberg, *Sci. Total Environ.*, 1994, **150**, 201–207.
31 M. De Boeck, M. Kirsch-Volders and D. Lison, *Mutat. Res., Fundam. Mol. Mech. Mutagen.*, 2003, **533**, 135–152.
32 M. L. Clark, R. L. Green, O. E. Johnson, P. E. Fanwick and D. R. McMillin, *Inorg. Chem.*, 2008, **47**, 9410–9418.
33 P. C. Lee and D. Meisel, *J. Phys. Chem.*, 1982, **86**, 3391–3395.
34 V. Giannini and J. A. Sanchez-Gil, *J. Opt. Soc. Am. A*, 2007, **24**, 2822–2830.
35 P. R. Andres and U. S. Schubert, *Adv. Mater.*, 2004, **16**, 1043–1068.
36 E. C. Constable, *Chem. Soc. Rev.*, 2007, **36**, 246–253.
37 H. Hofmeier, R. Hoogenboom, M. E. L. Wouters and U. S. Schubert, *J. Am. Chem. Soc.*, 2005, **127**, 2913–2921.
38 C. H. H. Traulsen, E. Darlatt, S. Richter, J. Poppenberg, S. Hoof, W. E. S. Unger and C. A. Schalley, *Langmuir*, 2012, **28**, 10755–10763.
39 G. J. Thomas and D. A. Agard, *Biophys. J.*, 1984, **46**, 763–768.
40 World Health Organization, *Cobalt and Inorganic Cobalt Compounds Concise International Chemical Assessment Document 69*, 2006.
41 R. Dobrawa, M. Lysetska, P. Ballester, M. Grune and F. Wurthner, *Macromolecules*, 2005, **38**, 1315–1325.
42 V. W. W. Yam, K. M. C. Wong and N. Y. Zhu, *J. Am. Chem. Soc.*, 2002, **124**, 6506–6507.
43 B. G. G. Lohmeijer and U. S. Schubert, *Angew. Chem., Int. Ed.*, 2002, **41**, 3825–3829.
44 A. Gasnier, J. M. Barbe, C. Bucher, C. Duboc, J. C. Moutet, E. Saint-Aman, P. Terech and G. Royal, *Inorg. Chem.*, 2010, **49**, 2592–2599.
45 Sustainable Water Group, Water Quality Guidelines, http://www.bsr.org/reports/awqwg/BSR_AWQWG_Guidelines-Testing-Standards.pdf, 2010.

